

Effects of microcrack-damage on fracture behavior of TiAl alloy. Part II: load-controlled tensile test

Rui Cao · Hao Zhu · Jian Hong Chen ·
Ji Zhang

Received: 19 December 2006 / Accepted: 17 September 2007 / Published online: 17 October 2007
© Springer Science+Business Media, LLC 2007

Abstract Specimens of a fully lamellar TiAl alloy and a duplex TiAl alloy were tensile tested using load-controlled procedure. The microcracks were measured for each specimen as it was subjected to various preloading–unloading processes. Loading–unloading–reloading processes of in-situ tensile tests were carried out in a scanning electron microscope (SEM). Effects of microcrack damage on the deformation and fracture behavior were evaluated. The following results of microcrack-damage on deformation and fracture behavior of TiAl alloy were found: (1) The apparent plastic elongation resulted mainly from plastic strain. The elongation caused by microcracks is negligible. (2) No appreciable effects of microcrack damage on the apparent elastic modulus could be found. (3) Microcracks damage produced at higher preloading reduced the fracture stress, however, that produced at lower preloading gave diminished effects.

Introduction

Many studies have been done to reveal the tensile fracture processes and fracture mechanisms of TiAl alloys [1–11].

R. Cao · H. Zhu · J. H. Chen
State Key Laboratory of Gansu Advanced Non-ferrous Metal
Materials, Lanzhou University of Technology,
Lanzhou 730050, China

R. Cao · H. Zhu · J. H. Chen (✉)
Key Laboratory of Non-ferrous Metal Alloys, The Ministry of
Education, Lanzhou University of Technology,
Lanzhou 730050, China
e-mail: zchen@lut.cn

J. Zhang
China Iron and Steel Research Institute Group,
Beijing 100081, China

In recent work [6], the numerical results demonstrated a subtle interplay between the microstructural geometry, the cohesive strengths, and the yield strength. For instance, when the yield strength was reduced, new damage modes appeared due to enhanced plastic deformation. Also, the colony boundary toughness determined a threshold toughness, at which a boundary crack would form in lieu of renucleation into an unfavorably oriented neighboring colony. Increasing the boundary toughness could defer such boundary cracks and thus permitted an increase in renucleation events and in the generation of the associated ductile ligaments. Decreasing the α_2 plane (or the α_2 – γ boundary) toughness could also increase renucleation, microcracking, and hence increase ligament toughening and other energy-dissipating phenomena [6]. In [12], damage behaviors of TiAl alloy under thermal fatigue and thermal cycling with Dead-Load are shown. During shorter thermal cycling, the damage parameter increased intensely, and the difference between D_E (modulus damage parameter) and D_R (electrical resistance damage parameter) was very limited. Then, the damage parameter increased very slowly as thermal cycling increased gradually. Finally, the damage parameter approached a constant, and the difference between the two damage parameters also became stable.

The effects of microcracks on the plastic deformation of a fully lamellar (FL) γ -TiAl alloy were investigated [13]. In the research, several results related to this article were obtained:

While the FL TiAl alloys deformed at relative low strain-controlling rates (1×10^{-5} /s), a large number of microcracks nucleated within the grains and lead to the following conclusions:

The apparent plastic elongation incorporates both plastic strain and the elongation caused by microcracks. Fracture

load decreases with increasing microcrack density. The larger the grain size, the higher the microcrack density, thus, higher the apparent plasticity and the lower the fracture stress.

In a previous article by the present authors [14], the effect of microcrack damage on fracture behavior was investigated using the procedure of displacement-controlled. Figure 1 shows the σ - ϵ curves drawn from procedures of loading-unloading-reloading at two levels of preload. Figure 2 summarizes the σ - ϵ curves drawn from procedures of reload-to-fracture preceded by various levels of preloading. On the basis of these figures, the effects were divided into two categories:

(1) Volumetric effects caused by microcracks produced in entire volume of a specimen:

(a) *Decreasing the apparent elastic modulus*

As seen in Fig. 1, the slopes of stress-strain curve (presenting the elastic modulus) of reloading processes are apparently less than those in preloading process. The loss of the elastic modulus was attributed to the elongation caused by the volumetric effect of microcrack damage.

(b) *Producing a stress-softening sector (stress dropping with strain increasing) on the load-displacement curve just before final fracture.*

The stress-softening sectors (stress dropping with strain increasing) on the load-displacement curves just before final fracture shown in Fig. 2 were also attributed to the elongation caused by the volumetric effect of microcracks. In these cases, the rate of crack-induced-elongation surpassed the rate of the crosshead of the testing machine, and the load dropped with increasing elongation of the specimen.

(2) Facial effects caused by microcracks produced on a weakest cross section:

Microcracks extended on a weakest cross section determine the fracture load. The more microcracks produced in the loading process, the lower the fracture stress. Since in spite of various preload procedures, similar quantities of microcracks were produced before the final

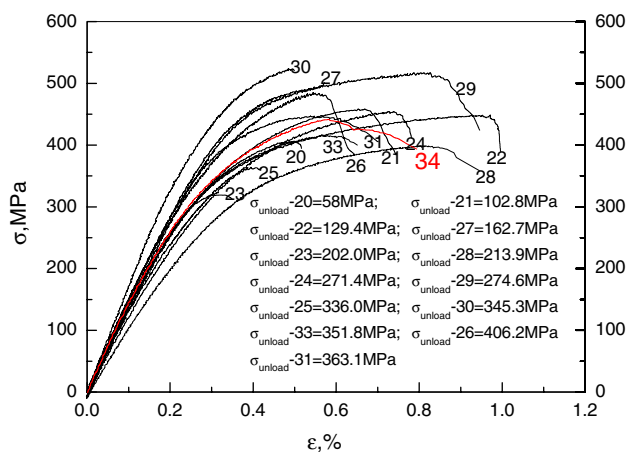


Fig. 2 Curves plotting applied stress against strains measured in tensile tests after various preload processes [14]

fracture, thus the fracture stresses of most specimens showed a value around 400 MPa.

These effects were analyzed as the results produced in the procedure of displacement (strain)-controlled mode. However, effects of microcrack-damage on fracture behavior of TiAl Alloy are not reported. What will happen in a procedure of load (stress)-control mode is the subject of this work. In present work, the authors combine loading-unloading-reloading tests using load-controlled procedure to identify effects of microcrack-damage on fracture behavior of TiAl Alloy.

Experimental procedures

Materials and specimens

A TiAl alloy with compositions shown in Table 1 was used. All samples were taken from a forged pancake that has been deformed at 1,100 °C for a 70% height reduction. Two types of microstructures, duplex (DP) and near fully lamellar (FL), were obtained as shown in Fig. 3. The

Fig. 1 Curves of stress-strain plotted for tension preloading-unloading-reloading fracture processes (a) preloading-unloading at 275 MPa, (b) preloading-unloading at 363 MPa [14]

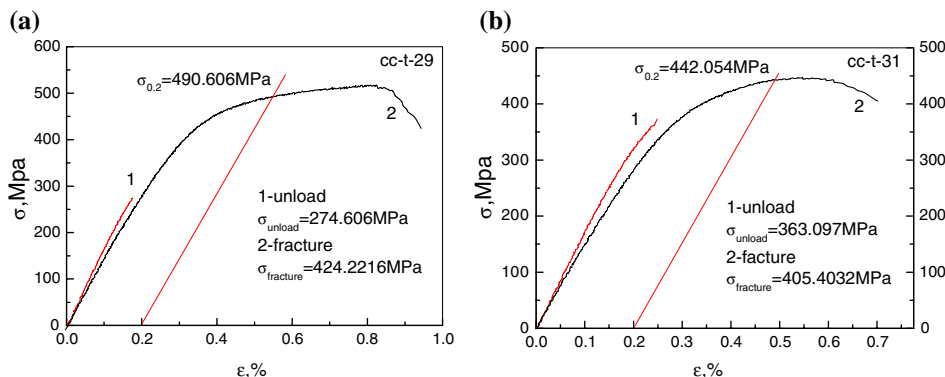


Table 1 Compositions of TiAl alloy (at %)

Ti	Al	V	Cr
Balance	47.5	2.5	1.0

samples were first wrapped in quartz tubes, treated by hot isostatic pressing in 950 °C, 120 MPa in Argon for 3 h and put into the furnace at pre-determined temperatures. DP microstructure samples were obtained by annealing at 1,250 °C for 18 h, and FL microstructure samples by annealing at 1,370 °C for 1 h.

The dimensions of flat tensile specimen are shown in Fig. 4(a) and all specimens were polished before testing. The dimensions of notched tensile specimens for in-situ observations are shown in Fig. 4(b). In Fig. 4(b), the thickness of the specimens was varied in the range of 0.20–1.1 mm. Two types of notches were cut, i.e., Chevron notch (45° V notch) with 250 μm in root radius, and slit notch having parallel sides (S notch) and 87 μm root radius. Specimens were cut by electric-spark machining (ESM), mechanically polished and then etched in a solution of 10% HNO₃, 3% HF, and 87% water.

Mechanical tests

Tensile tests were conducted in air at room temperature using INSTRON1341 test machine with a loading speed of 150 N/min. Values for yield stress ($\sigma_{0.2}$), ultimate tensile strength (σ_{uts}), fracture strain (ϵ_f), fracture stress (σ_f), and elastic modulus (E) were measured from engineering stress–strain curves of the tensile test data. All stress values were defined as the quotients of the corresponding load divided by the original section area. The elastic modulus,

E, was defined as the quotient of stress divided by strain in the elastic region.

Preloading–unloading–reloading procedure

Tensile test specimens were processed using a repetitive tensile preloading–unloading procedure at various applied loads with a loading speed of 150 N/min. Some specimens were reloaded to fracture after repeated loading–unloading procedure at various levels of preloads. Stress–strain curves were plotted from the test data of tensile preloading–unloading and reloading to fracture tests.

Measurement of microcrack densities

Four metallographic sections parallel to the tensile direction were cut from each specimen subjected preload at various levels and then polished and slightly etched. The numbers of microcracks were measured on the metallographic surface divided into areas with 3 mm × 4 mm in size. The density of microcracks was taken as a statistic index of damage.

In-situ observation of tensile tests in SEM

In situ tensile tests were performed under vacuum using a calibrated loading stage mounted in a scanning electron microscope (SEM) S-520. The specimens were exposed to processing by which they were slowly step-loaded–unloaded–reloaded manually, and the crack patterns at various loading or unloading steps were recorded by SEM. The crack initiating and propagating processes in conjunction with applied loads were recorded.

Fig. 3 Microstructures of (a) fully-lamellar, (b) Duplex TiAl-based alloy

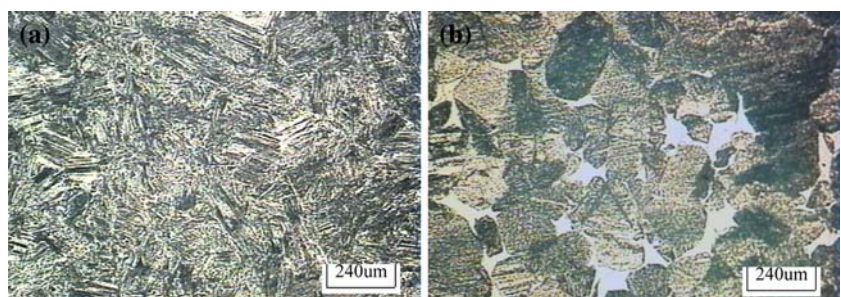
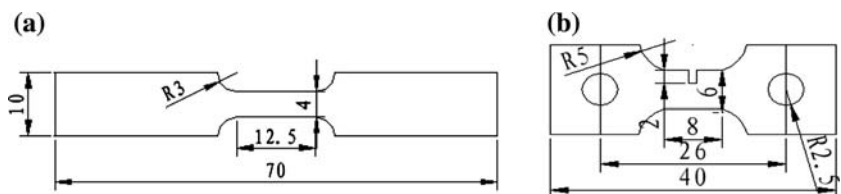


Fig. 4 Dimensions of specimens for (a) tensile tests, (b) in-situ observations (mm)



Observations of fracture surfaces

Fracture surface observations were carried out by SEM on all fractured specimens with or without tensile preload–unload procedures. In addition to the general pattern for whole fracture surface, attention was focused on the inter-lamellae-fracture facets. From the direction of crack propagation on fracture facets, it was possible to distinguish which one was fractured before the final fracture and which one was fractured at the final fracture. The facets, which are fractured at the final fracture showed direction of crack propagation, and formed a link of a chain. This chain oriented from the crack initiation site and extended to the fracture end. Most facets, fractured before the final fracture, were inter-lamellar and did not show appreciable cracking directions. The areas of these facets were also taken as a damage parameter.

Fracture surface observations of in-situ tensile specimens were carried out along the path of surface crack extension. By measuring and designating the distances from the notch root to the surface cracks, and the distance to the fracture facets, the fracture facet could be related in a one-to-one fashion to the sector of surface crack.

Experimental results

Results of repeatedly preload–unload–reload processes

Figures 5 and 6 show the σ – ε curves of repeatedly preloading–unloading–reloading processes with various

preloading levels for full lamellar (FL) alloy and duplex (DP) alloy samples, respectively. From Figs. 5 and 6 two ideas are drawn: (1) For both FL and DP alloys, no difference in the elastic modulus was found between preload and reload procedures. It means that opposite to the case of a displacement-controlled mode (Fig. 1), in a stress-controlled mode, there is no effect due to preload on the elastic modulus of TiAl alloy. (2) After the preload reached 194 MPa non-reversible strain was produced and remained even after unloading. In the reload procedure, the non-reversible strain did not increase until the applied load reached the value of unloading. The profile of the entire loading process shows a smooth curve, which is typical behavior of plastic deformation. Both phenomena indicate that the non-reversible displacement is mainly that of plastic displacement.

Results of fracture-loading procedures preceded by repeated preload–unload–reload

Figure 7(a) and (b) show the σ – ε curves which were drawn during the fracture-loading tests of FL and DP TiAl alloys after various repeated preload–unload–reload processes. Tables 2 and 3 summarize results of tensile-fracture tests. In Tables 2 and 3, fracture stresses, fracture strains, and yield stresses measured in tensile tests after various repeated preload–unload–reload processes are also listed along with the preloads. From Table 2 and Fig. 7(a), the following events were found for FL alloys: When the unloading stress is less than 197.43 MPa, no appreciable

Fig. 5 σ – ε curves of repeatedly preload–unload–reload processes of specimens (a) tensile fracture specimen FL-T-3 after preloading at 33 MPa, (b) tensile fracture specimen FL-T-9 after preloading at 33 MPa, reloading at 65 and 194 MPa, (c) tensile fracture specimen FL-T-13 after preloading at 32 MPa, reload at 64, 192, 319, and 383 MPa, (d) tensile unloading specimen FL-T-12 after preloading at 32 MPa, reloading at 64, 192, 320, 384, and 448 MPa

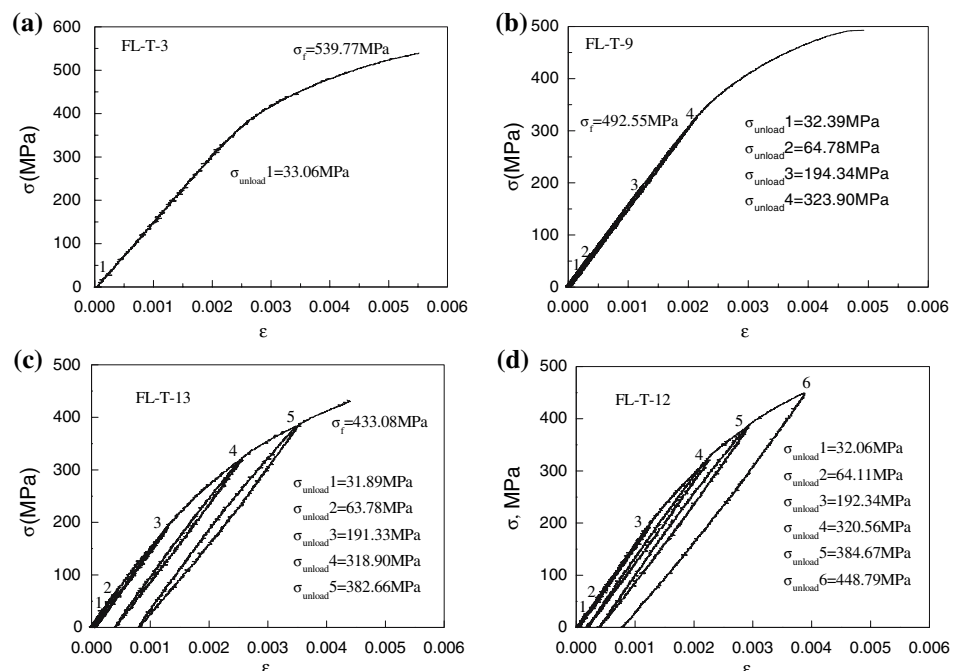


Fig. 6 σ – ε curves of repeated preload–unload–reload processes of specimens (a) tensile fracture specimen DP-T-4 after preloading at 32 MPa, (b) tensile fracture specimen DP-T-10 after preloading at 33 MPa, reload at 65, 195, and 326 MPa, (c) tensile fracture specimen DP-T-13 after preloading at 33 MPa, reloading at 65, 196, 327, and 392 MPa, (d) tensile unloading specimen DP-T-14 after preloading at 33 MPa, reloading at 65, 196, 327, 393, and 419 MPa

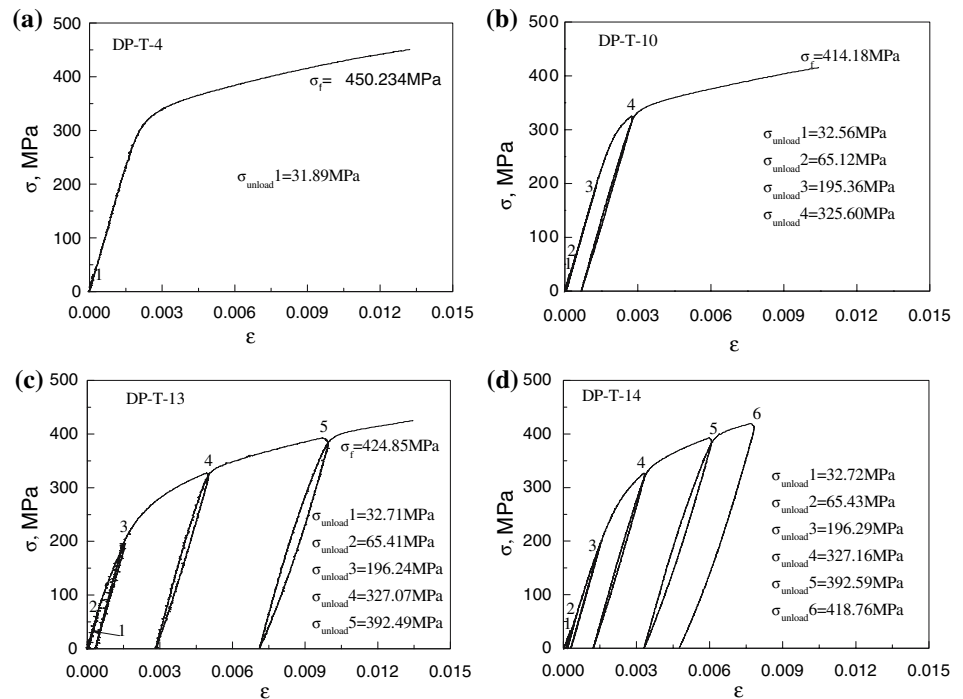
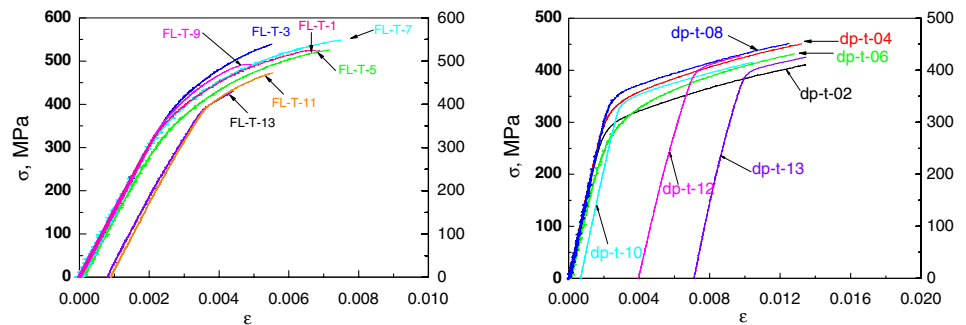


Fig. 7 Curves plotting applied stress against strains measured in tensile fracture tests after various repeatedly preload–unload–reload processes



changes appear in fracture stress (σ_f), fracture strain (ε_f), and fracture energy per unit areas (w_f). When the unloading stress is higher than 197.43 MPa, these properties (σ_f , ε_f , and w_f) appreciably decrease with increase in the preload. From Table 3 and Fig. 7(b) for DP alloys, when the unloading stress reaches 325.60 MPa, the fracture stress (σ_f), fracture strain (ε_f), and fracture energy per unit areas (w_f) show a weak decreasing tendency with increasing the preload.

For both fully lamellar and duplex TiAl alloys, there no a stress-softening sector (stress dropping with strain increasing) appeared in the σ – ε curves.

In summary, in contrast to the displacement-controlled loading mode, in tests using load-controlled loading mode, the volumetric effects of microcrack damage (i.e., loss of elastic modulus and production of a stress-softening sector (stress dropping with strain increasing) on the σ – ε curve)

were not present. However, the facial effects of damage from microcracks were present, which decreased the fracture stress.

Results of microcrack measurements

Tables 4 and 5 show statistical results of crack measurement in tensile preloading–unloading tests of FL and DP TiAl alloys. From Table 4, for the FL alloy crack densities show an appreciable increase with increasing unloading stress (except specimen FL-T-12). However, for the DP alloy with a much smaller grain size no regular change was found in crack densities with increasing unloading stress. Figures 8 and 9 show crack distributions on metallographic surfaces of specimens unloaded at various applied loads for both FL and DP alloys. These figures corroborate the

Table 2 Results of Tensile-Fracture Tests of FL TiAl alloys after various repeated preload-unload-reload processes at different preload conditions

Specimens	S_e (mm ²)	σ_{unload} (MPa)	σ_f (MPa)	$\sigma_{0.2}$ (MPa)	ε_f	w_f (J/mm ²)
FL-T-1	1.92*4.00	0	524.38	484.65	0.00689	0.0316
FL-T-3	1.90*3.98	33.06	539.77	529.76	0.005438	0.0236
FL-T-5	1.92*4.02	32.39, 64.78	525.81	467.78	0.007135	0.0319
FL-T-7	1.89*4.00	32.90, 65.80, 197.43	547.63	490.40	0.007452	0.0359
FL-T-9	1.92*4.00	32.39, 64.78, 194.34, 323.90	492.55	–	0.004925	0.0196
FL-T-11	1.94*4.02	32.39, 64.78, 194.34, 323.90, 388.68	471.93	–	0.005514	0.0175
FL-T-13	1.96*4.00	31.89, 63.78, 191.33, 318.88, 382.65	433.08	–	0.004351	0.0111

S_e = true area of original cross section, σ_{unload} = unload stress, σ_f = fracture stress, ε_f = fracture stress, $\sigma_{0.2}$ = yield stress, w_f = fracture work per unit areas

Table 3 Results of tensile-fracture tests of DP TiAl alloys after various repeated preload-unload-reload processes at different preload conditions

Specimens	S_e (mm ²)	σ_{unload} (MPa)	σ_f (MPa)	$\sigma_{0.2}$ (MPa)	ε_f	w_f (J/mm ²)
DP-T-2	1.94*4.0	0	409.80	325.39	0.01342	0.0549
DP-T-4	1.96*4.0	31.89	450.23	360.26	0.01319	0.0595
DP-T-6	1.96*4.0	31.89, 63.78	431.58	328.80	0.01274	0.0533
DP-T-8	1.92*4.02	32.39, 64.78, 194.34	451.33	375.77	0.01247	0.0568
DP-T-10	1.92*4.0	32.56, 65.12, 195.36, 325.60	414.18	367.95	0.01043	0.0406
DP-T-12	1.94*3.92	32.71, 65.42, 196.26, 327.10, 392.52	426.98	422.45	0.00973	0.0221
DP-T-13	1.94*3.94	32.71, 65.41, 196.24, 327.07, 392.49	424.85	417.36	0.01345	0.0255

S_e = true area of original cross section, σ_{unload} = unload stress, σ_f = fracture stress, ε_f = fracture stress, $\sigma_{0.2}$ = yield stress, w_f = fracture work per unit areas

Table 4 Crack statistical results of tensile preload-unload tests of FL TiAl alloys

Specimens	S_e (mm ²)	σ_{unload} (MPa)	Average surface-crack density	Average inter-crack density	Total average crack density
FL-T-2	1.96*4.04	31.57	21.00	19.60	20.30
FL-T-4	1.92*4.00	32.55, 65.10	27.01	30.00	28.51
FL-T-6	1.94*4.04	31.90, 63.80, 191.39	63.94	17.37	40.66
FL-T-8	1.92*4.00	32.55, 65.10, 195.31, 325.52	35.87	40.54	44.31
FL-T-12	1.94*4.02	32.06, 64.11, 192.34, 320.56, 384.67, 448.79	50.61	5.22	27.92

Table 5 Crack statistical results of tensile preload-unload tests of DP TiAl alloys

Specimens	S_e (mm ²)	σ_{unload} (MPa)	Average surface-crack density	Average inter-crack density	Total average crack density
DP-T-3	1.96*4.02	31.73	22.47	8.05	15.26
DP-T-5	1.92*3.98	32.72, 65.43	14.20	2.39	8.30
DP-T-7	1.92*3.96	32.88, 65.76, 197.29	24.12	7.91	16.02
DP-T-9	1.94*3.96	32.54, 65.08, 195.25, 325.42	29.97	8.76	19.37
DP-T-11	1.92*3.96	32.88, 65.76, 197.29, 328.81, 394.57	13.51	9.64	11.58
DP-T-14	1.92*3.98	32.72, 65.43, 196.29, 327.16, 392.59, 418.76	12.57	17.93	21.47

Fig. 8 Metallographic surfaces of specimens unloaded at various applied loads for FL alloys (a) 31.57 MPa, (b) 31.90, 63.80, and 191.39 MPa

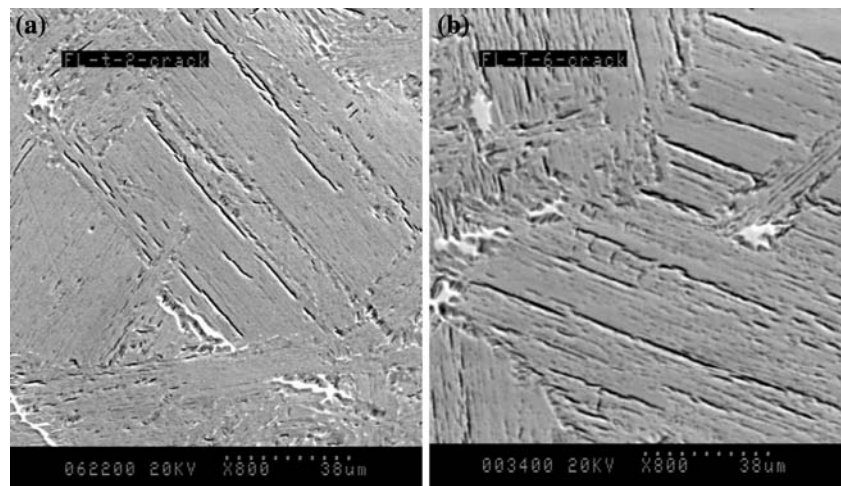
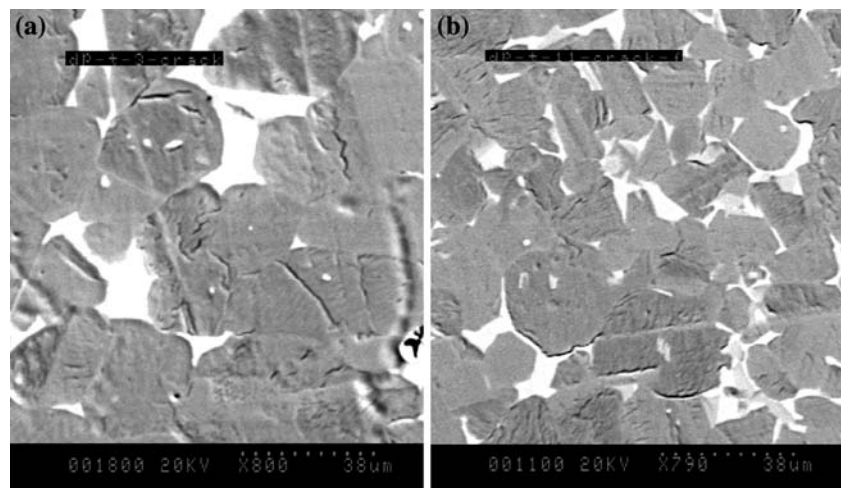


Fig. 9 Metallographic surfaces of specimens unloaded at various applied loads for DP alloys (a) 31.73 MPa, (b) 65.76, 197.29, 328.81, and 394.57 MPa



tendency of changes in crack densities listed in Tables 4 and 5.

Result of Observations of Fracture Surfaces

Figure 10 shows fracture surface of specimen FL-T-11 with repeatedly preload–unload–reload procedures. It is found that main crack initiated from facets with areas $250 \times 250 \mu\text{m}$ at top right of the fracture surface (Fig. 10a). A close view with a higher magnification is shown in Fig. 10(b). The initiated crack propagates in a distinct direction as shown by Fig. 10(c) and (d). A series of cleavage facets with distinct directional river patterns propagated from the initiating facet. These cleavage facets were apparently cleaved at the last moment of final fracture when the crack extended through the remaining ligament of the specimen.

Since there is no distinct direction of crack propagation on facets, where the initiating main crack initiated (Fig. 10b), these facets and some similar facets around were considered to be produced during the preload–reload procedures before the fracture. In Fig. 10(e), a large facet without distinct crack propagation direction was also produced during preload–reload procedures. The areas of cracks produced before the final fracture account for about several percentage of the total fracture surface.

For the DP alloy, the facets presented on the fracture surface are much finer than those of FL alloy. However, facets can still be characterized by the surface veins; with the direction of crack propagation and without it. Figure 11 shows fracture surface of specimen DP-T-10 after repeated preload–unload–reload process, it was found that a crack initiates from region A (by arrow) in Fig. 11(a). A close view of Region B in Fig. 11(a) is shown by Fig. 11(b).

Fig. 10 Fracture surface of specimen FL-T-11 preloaded at 33 MPa, unloaded to 0 MPa, reload at 65, 194, and 324 MPa

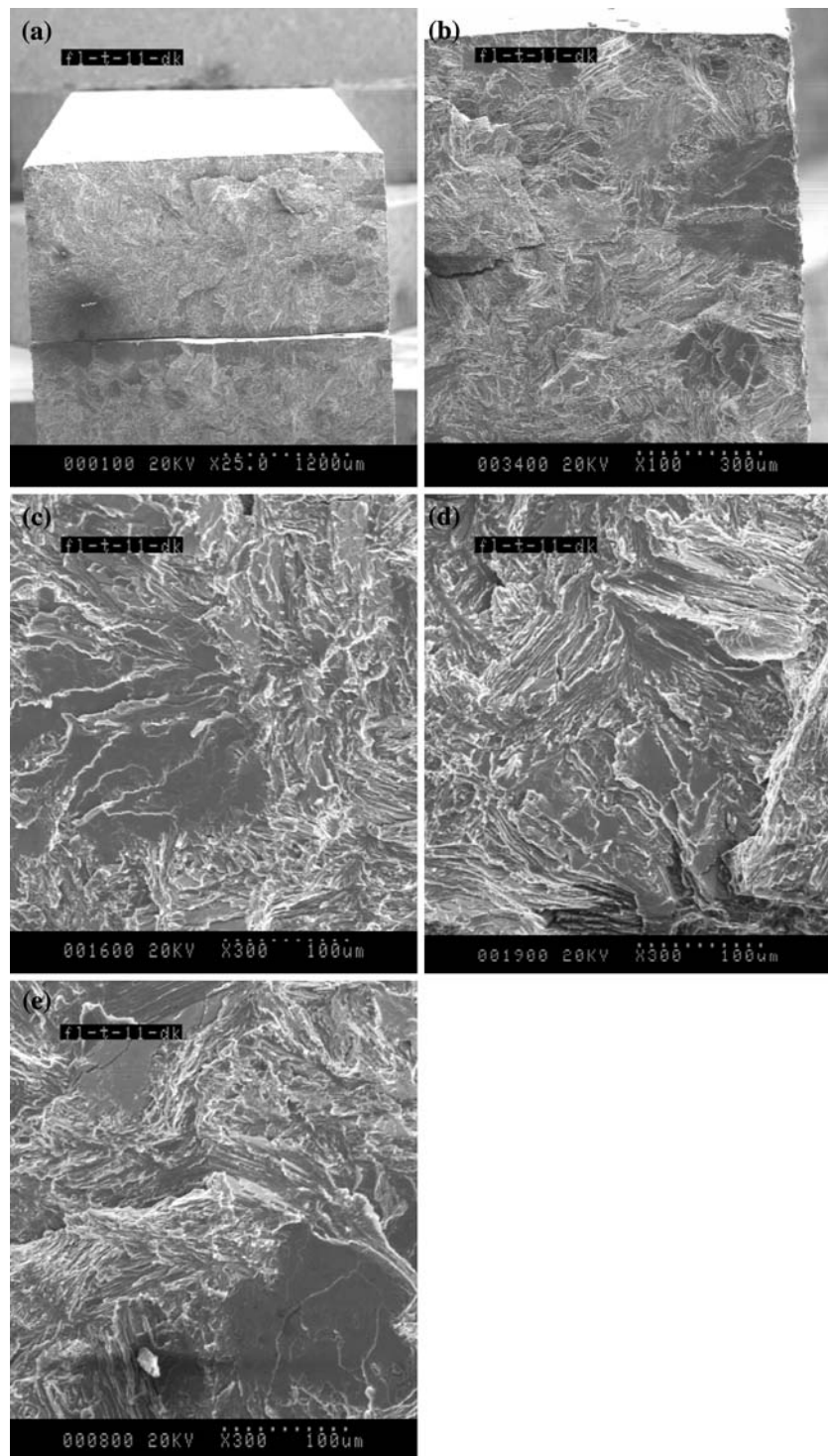


Figure 11(c) shows some facets of 20–30 μm in size without distinct directional crack propagation, which were produced in preload and reload procedures. Figure 11(d–f) shows a series of cleavage facets with directional river patterns appearing in the fracture surface, which were produced in the final fracture.

Results of in-situ observations

Figure 12(a) shows the plot of applied load versus the main crack length and the patterns of main crack at several steps of loading (Fig. 12b–e). As seen in Fig. 12(c), many microcracks were produced between two

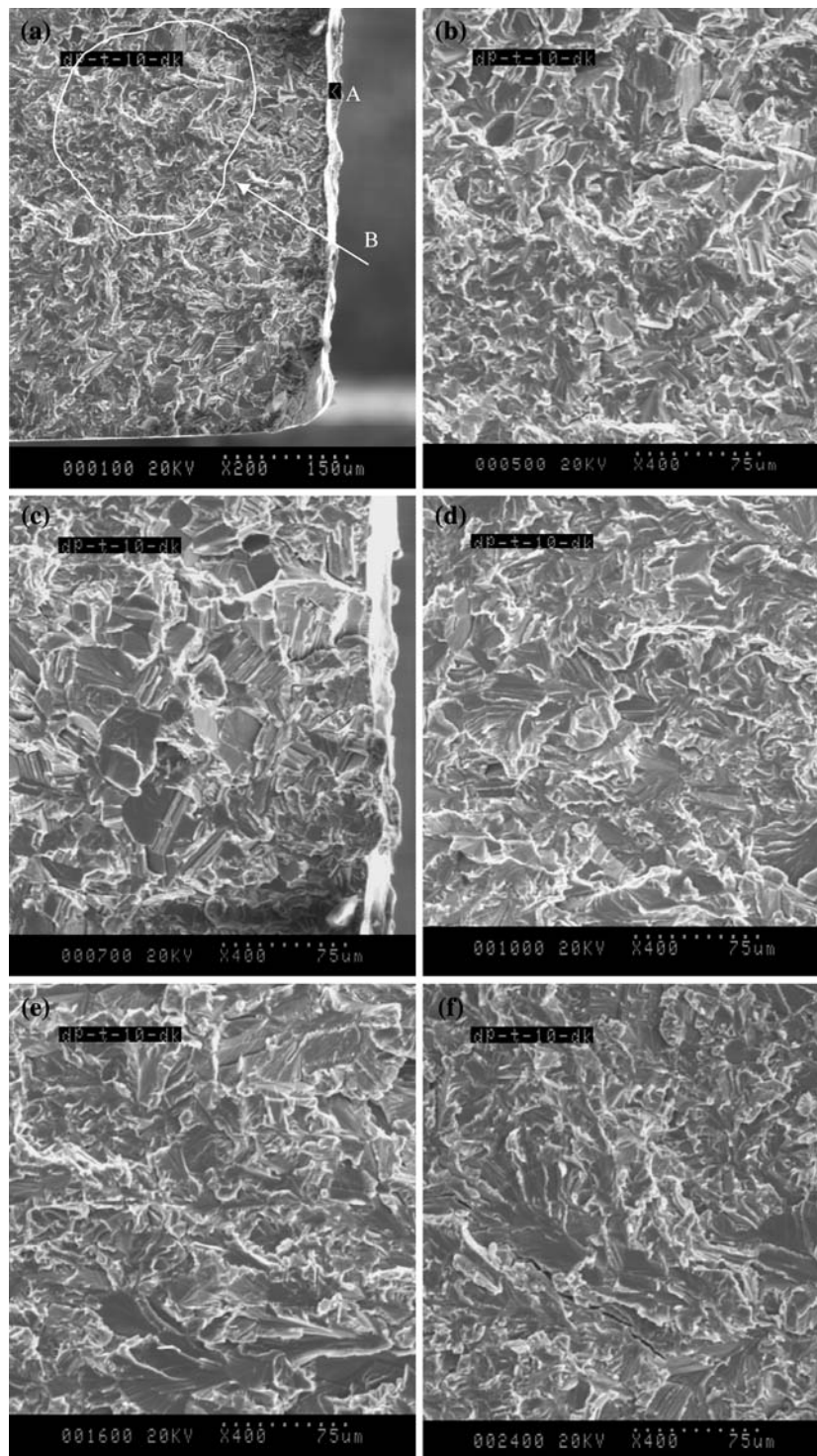
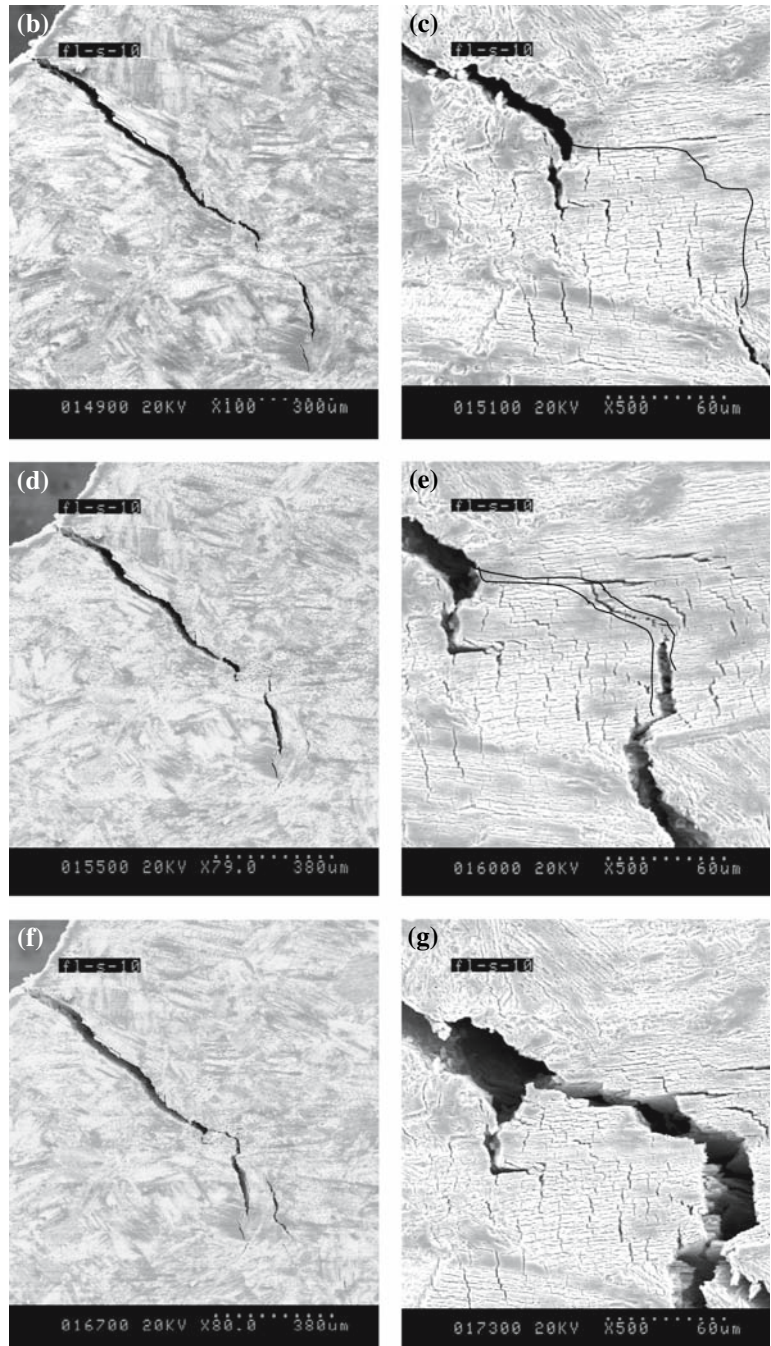
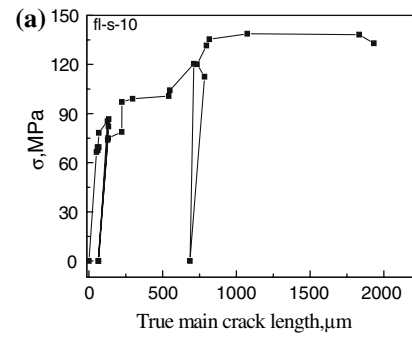


Fig. 11 Fracture surface of specimen DP-T-10 preloaded at 33 MPa, unloaded to 0 MPa, reload at 65, 195, and 326 MPa

separate sectors of the main crack (Fig. 12b). However, in the final path (indicated by the black envelope line) the upper sector of the main crack by-passed the high microcrack density region and propagated along the

lamellar boundary first, then connected with the bottom sector by a translamellar crack (Fig. 12d and e). From Fig. 12(a), no effect on the load curve was found due to these microcracks.

Fig. 12 Results of in-situ observations of specimen fl-s-10. Curves plotting applied stress σ against the lengths of main crack L (a), crack patterns corresponding to the crack propagation curve of fl-s-10 in (a) at various applied stress: 124.60 MPa (b), 124.16 MPa (c), 128.27 MPa (d), 127.53 MPa (e), 131.50 MPa (f), 126.95 MPa (g)



Discussion

Reason why the volumetric effects of microcrack damage are not notable in a load (stress)-controlled mode

As mentioned in “Results of repeatedly preload–unload–reload processes” section, there was no appreciable loss in elastic modulus and no stress-softening sector (stress dropping with strain increasing) on the σ – ε curves in tensile tests using a load-controlled mode. The reason for these phenomena is analyzed as follows:

- (1) In a load-controlled loading mode, the rate of increasing the applied load is kept constant by the test machine regardless of the changes in deformation (elongation). Therefore, it is impossible for a stress-softening sector (stress dropping with strain increasing) to be produced on the σ – ε curves like in the case of a displacement-controlled loading mode.
- (2) In a load-controlled mode with a higher crosshead rate, the microcracks would have been barely produced and insufficiently developed. In Table 4 for a FL alloy, the tendency of increased crack density with increasing preload and reload is appreciable, but not remarkable.
- (3) For a DP alloy with fine grains, the volumetric effects are further weakened due to the shorter lengths of microcracks confined within the fine grains. Moreover, in a fine grain microstructure, it is more difficult to produce microcracks. This idea is corroborated by Table 5, which shows that no regular change is found in crack densities with increased unloading stress.
- (4) The weak volumetric effects of microcracks identify that the non-reversible strain produced in preload and reload processes is mainly composed of the plastic strain and little of the elongation, which is caused by microcracks.

Reason why the facial effects of microcrack damage are appreciable in a load (stress)-controlled mode

As mentioned above, microcracks would have been barely produced and insufficiently developed in a load-controlled mode. Therefore, the question is: why did the fracture stress decrease more appreciably than that in a displacement-controlled mode with increasing the preload. The following explanations are likely:

- (1) When using a displacement-controlled loading mode, in spite of various preload procedures, the fracture stresses of most specimens show a value around

400 MPa. This is because both the preload and the fracture-loading processes follow a similar loading route. Therefore, the differences in the numbers of cracks produced by various preloading processes are compensated during the fracture loading process. Thus, similar quantities of microcracks were produced before the final fracture. This process gives the false impression that no effects are caused by various preload conditions on the fracture stress. In fact, the facial effects of microcrack damage on decreasing the fracture stress do present, however, as shown in Fig. 2 a stress-softening sector (stress dropping with strain increasing) on σ – ε curve makes up the difference and gives the fracture stresses around 400 MPa for most specimen.

- (2) When using a load-controlled loading mode, microcracks would have been barely produced even in the final fracture loading process. There is no a stress-softening sector on the σ – ε curve. In this case, the different microcrack damages caused by various preload and reload procedures can not be compensated for in the final fracture loading process and show their appreciable effects on the fracture stress of the FL alloy (Table 4). Comparing with the FL alloy, the DP alloy shows less effects due to the fact that fewer cracks were produced (Table 5).
- (3) Although the total amount of microcracks produced in the load controlled loading process is not high, the microcracks concentrated in some of the weakest cross sections, which made the fracture stress lower. Figure 10 just shows this case, in which a number of cracks were produced in a cross section of specimen FL-T-11 before final fracture, making the fracture stress 10% lower than the average value (Table 4).

Differences in production of microcracks by a displacement-controlled tensile mode and by a load-controlled tensile mode

The differences in effects of damage caused by preload and reload processes between the displacement-controlled tensile mode and the load-controlled tensile mode is based on the difference in the production of microcracks during these two processes. The reason is analyzed as follows:

It was found by in-situ observation that at a fixed position of loading stage, some new microcracks were initiated and some cracks were extended. This means that the production of microcracks in TiAl alloy is time-delayed.

In a displacement-controlled mode, the elongation caused by the volumetric effects of new cracks and crack

extensions reduces the real elongation of the specimen's material and then reduces the rate of tensile load increment. In a process of slow increase in tensile load, and even of a decreasing load (producing the stress-softening sector on the σ - ε curve), microcracks develop sufficiently until a saturated condition is reached. The final fracture occurs at a balance between a low applied load and a low remaining cross section area. It is inferred that a higher controlled deformation rate will also reach a balance between a higher applied load and a higher remaining cross section area (because the higher load rate has barely produced lower density of cracks). It results in a higher fracture stress σ_f .

In a load-controlled mode, the production of cracks decreases the real cross section area, thus increases the real stress on the specimen material rather than decreases it. The real stress is raised at a rate higher than originally set and no stress-softening sector can be produced. In this case, the cracks would have been barely produced. It is inferred that higher the rate of increasing load, lower the density of microcracks and higher the fracture stress.

Effects of microcrack damage in a notched specimen

As mentioned in a previous article [15] the fracture behavior in a notched specimen is different from that in a smooth tensile test specimen. In a notched specimen, the main crack propagation is confined to a narrow strip extending in front of the notch where the normal stress is higher. In microscopic scale, the crack prefers to propagate through the lamellar boundary as an interlamellar crack. In a smooth tensile test specimen, the fracture occurs on a weakest cross section where the density of microcracks is highest. Figure 12 shows a crack resistance curve of specimen fl-s-10 (dimensions of specimen fl-s-10 are shown by Fig. 4(b), specimen's depth is 0.38 mm) and series of crack patterns of fl-s-10 at various extension steps corresponding to the crack propagation resistance curve in Fig. 12(a). As seen in Fig. 12, although a lot of microcracks are produced in a region between two separated sectors of the main crack, in the final path (indicated by the black envelope line) the upper sector of the main crack by-passes the high microcrack density region and propagates along the lamellar boundary first, and then connects with the bottom sector by a translamellar crack (Fig. 12f and g). From Fig. 12(a), no effect of these microcracks in the loading curve was found.

The reasons are analyzed as follows:

- (1) The cracks are surface cracks, so the effects are much weaker.
- (2) The main crack prefers to propagate along the lamellar boundary rather than to propagate in a region with high crack density. It means that the

resistance of lamellar boundaries is lower than the region of cracks of high density, most of which are of translamellar cracks.

- (3) The loading curve is mainly determined by the resistance to the main crack propagation, no effects of microcracks on the loading curve result and no effects of these microcracks on the main crack propagation could be identified.

In summary, in the notched specimens the effects of microcrack damage is less than that in the smooth tensile test specimens.

Conclusions

On the basis of tensile tests using load-controlled procedure of specimens of a fully lamellar TiAl alloy and a duplex TiAl alloy, and measurement of numbers of microcracks produced in various preload-unload processes, effects of microcrack damage on the displacement and fracture behavior are summarized as follows:

- (1) The apparent non-reversible elongation in smooth tensile test specimens results mainly from plastic strain. The elongation caused by microcracks is negligible.
- (2) In load-controlled mode tests, the volumetric effects of microcrack damage are unappreciable. No appreciable effects of microcrack damage on the apparent elastic modulus could be found. No stress-softening sector (stress dropping with increasing strain) appears on the σ - ε curve, which is caused by microcrack damage and appears in the displacement-controlled mode tests.
- (3) In load-controlled mode tests, the facial effects of microcrack damage are appreciable: Microcrack damage produced by high preload on a weakest cross section reduced the fracture stress.

Acknowledgements This work was financially supported by the National Nature Science Foundation of China (No. 50471109) and Nature Science Foundation of GanSu Province (No. 3ZS061-A25-037). Authors express their sincere gratitude to Ms. Ello for her help in language editing.

References

1. Chan KS, Kim YW (1992) Metall Trans 23A:1663
2. Chan KS, Onstott J, Kumar KS (2000) Metall Mater Trans 31A:71
3. Inui H, Oh MH, Nakamura A, Yamakuchi M (1992) Acta Mater 40:3095
4. Chan KS, Shih DS (1997) Metall Mater Trans 28A:79
5. Campbell JP, Kruzic JJ, Lillibridge S, Venkateswara Rao KT, Ritchie RO (1997) Scripta Mater 37:707

6. Arata JJM, Kumar KS, Curtin WA, Needleman A (2001) *Inter J Fract* 111:163
7. Arata JJM, Kumar KS, Curtin WA, Needleman A (2002) *Mater Sci Eng A* 329–331:532
8. Bowen P, Chave RA, James AW (1995) *Mater Sci Eng* 192/193A:443
9. Mercer C, Soboyejo WO (1997) *Acta Mater* 46:4385
10. Kad BK, Dao M, Asaro RJ (1995) *Phil Mag* 71A:567
11. Frank GJ, Olson SE, Brockman RA (2003) *Intermetallics* 11:331
12. Li J, Qiao S, Han D, Li M (2007) *Mater Sci Eng A* 471:106
13. Zheng RT, Zhang YG, Chen CQ (2004) *J Mater Sci* 39:1721
14. Cao R, Zhu H, Chen JH, Zhang J, Yao HJ (2007) *Mater. Sci. Eng. A*, in press
15. Chen JH, Cao R, Wang GZ, Zhang J (2004) *Mater Mater Trans* 35A:439